Medicinal Chemistry Research
https://doi.org/10.1007/s00044-020-02666-6

MEDICINAL CHEMISTRY RESEARCH

ORIGINAL RESEARCH

Design, synthesis and biological evaluation of Schiff's base derivatives as multifunctional agents for the treatment of Alzheimer's disease

Jian Shi[1] · Yi Zhou[1] · Keren Wang[1] · Qinge Ma[2] · Rongrui Wei[2] · Qingfeng Li[3] · Yiyang Zhao[1] · Zhanpin Qiao[1] · Shuang Liu[1] · Yumin Leng[4] · Wenmin Liu[1] · Zhipei Sang[1]

Received: 26 August 2020 / Accepted: 5 November 2020

Abstract

A series of Schiff's base derivatives was rationally designed, synthesized, and evaluated as multi-function agents for the treatment of Alzheimer's disease (AD). The results revealed that compound **3b** was a novel multifunctional agent. It acted as a highly selective monoamine oxidase-B inhibitor ($IC_{50} = 8.4$ nM), which was explained by the docking study. Compound **3b** also was an antioxidant agent (2.3 eq) and could significantly inhibit self-induced $A\beta_{1\text{-}42}$ aggregation (31.8%). Meanwhile, compound **3b** was a selective metal chelator and could inhibit Cu^{2+}-induced $A\beta_{1\text{-}42}$ aggregation (62.3%). Furthermore, compound **3b** presented good neuroprotective effects on H_2O_2-induced PC12 cell injury. More importantly, compound demonstrated good blood brain barrier permeability and druglike properties. Therefore, compound **3b**, a promising multi-targeted active molecule, offers an attractive starting point for further study in the drug-discovery process against AD.

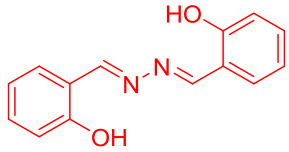

3b

MAO-B, IC_{50} = 8.4 nM; Antioxidant activity;
Self-induced Aβ aggregation: 31.8% inhibition rate
Cu^{2+}-induced Aβ aggregation: 62.3% inhibition rate
Selective metal chelator; neuroprotective agent;
Good BBB permeability and drug-like properties.

These authors contributed equally: Jian Shi, Yi Zhou

Supplementary information The online version of this article (https://doi.org/10.1007/s00044-020-02666-6) contains supplementary material, which is available to authorized users.

✉ Yumin Leng
yumin_leng@126.com

✉ Wenmin Liu
liuwm1969@163.com

✉ Zhipei Sang
sangzhipei@126.com

[1] College of Chemistry and Pharmaceutical Engineering, Nanyang Normal University, Nanyang 473061, China

[2] State Key Laboratory of Innovative Drugs and High Efficiency Energy Saving and Consumption Reduction Pharmaceutical Equipment, Jiangxi University of Traditional Chinese Medicine, Nanchang 330004, China

[3] Foreign Languages School, Nanyang Normal University, Nanyang 473061, China

[4] College of Physics and Electronic Engineering, Nanyang Normal University, Nanyang 473061, China

Published online: 25 November 2020

Keywords Alzheimer's disease · Schiff's base derivatives · Multifunctional agents · Blood barrier permeability · Drug-like property

Introduction

Alzheimer's disease (AD) is a neurodegenerative disease, which is the most common form of dementia, characterized by memory disorders, behavioral disorders, and other cognitive impairments. It is estimated that more than 50 million people suffering from dementia globally nowadays and the figure will be 152 million by 2050 [1]. A heavy economic burden has been brought by the enormous expense to the family of patients, which may trigger serious socio-economic problems [1]. Numerous efforts have been made in exploring the mechanism of AD, and four acetylcholinesterase inhibitors (such as tacrine, donepezil, galantamine, and rivastigmine) and one *N*-methyl-D-aspartate receptor antagonist (memantine) had been approved by the food and drug administration for the treatment of AD patients. During the period of long-term clinical use, these drugs are effective in controlling the AD symptoms to a certain extent, but they cannot stop, prevent, or reverse the progression of AD [2].

Due to the multifactorial pathogenesis of AD, the multifunctional agents, possessing two or more complementary biological activities, have been regarded as the best pharmacological option [3–5]. In addition, several multitarget-directed ligand strategy (MTDLs) candidate drugs now reach the testing stage in clinical trials [6, 7].

The amyloid hypothesis states that accumulation of amyloid-β (Aβ) is the triggering event in the pathogenesis of AD and it is prone to aggregate into oligomers, which leads to the damage and death of neurons. In addition, accumulation of Aβ in the brain triggers the spread of tau-related neurofibrillary tangles, neuroinflammation, and neuronal degeneration and death, causing AD [8, 9]. Thus, inhibiting accumulation of Aβ oligomers in the brain will be beneficial in managing AD.

Metal ion hypothesis states that high levels and dysregulation of metal ions (such as Cu^{2+}, Fe^{2+}, and Zn^{2+}) are observed in the AD brains, accelerating formation of amyloid plaques as well as neurotoxic oxidative processes. Cu^{2+} and Zn^{2+} induce the generation of toxic Aβ oligomers by binding to Aβ peptides, and the redox-active metals, Cu(I/II) and Fe(II/III), generate cytotoxic reactive oxygen species and cause neuronal damage. So, biometal chealtors would be a potential therapeutic strategy for treating AD [10, 11].

Increasing evidence suggests that levels of monoamine oxidase-B (MAO-B) activity could increase up to threefold in the temporal, parietal, and frontal cortex of AD patients. The excess MAO-B produces hydroxyl radicals, which could increase the former of Aβ plaques [12]. Recently, selective inhibition of MAO-B has been acted as a potential approach for treating AD. Rasagiline is a selective MAO-B inhibitor, which has been approved for treating symptoms of Parkinson's disease [13]. Rasagiline has been performed a phase 2 trial in people with mild-to-moderate AD, and it significantly improves on the Quality of Life-AD test, and displays trends to better performance https://www.alzforum.org/therapeutics/rasagiline.

Schiff's base is a privileged skeleton, the Schiff's base derivatives as multifunctional agents have been widely investigated for the treatment of AD, such as selective MAO-B inhibitor, cholinesterase inhibitors, antioxidants, and modulators of Cu^{2+}-mediated Aβ aggregation [14–18]. Moreover, Clioquinol is a zinc and copper chelator, which would prevent Aβ accumulation and reduce brain amyloid deposition. The phase 2 trial of Clioquinol in patients with moderate to severe AD presents a beneficial cognitive https://www.alzforum.org/therapeutics/clioquinol. Herein, the chelation fragment of Clioquinol is fused into Schiff's base skeleton based on the MTDLs strategy to obtain a novel series of Schiff's base derivatives (Fig. 1), hoping these derivatives could be promising multifunctional agents possessing Aβ inhibitory activity, selective MAO-B inhibitory potency, antioxidant activity, metal chelation property, and anti-inflammation activity.

Results and discussion

Chemistry

The synthetic of 17 Schiff's base derivatives were depicted in Scheme 1. Briefly, the excessive amounts of benzaldehyde derivatives (benzaldehyde, **1a**; salicylaldehyde, **1b**; 4-hydroxy-3-methoxybenzaldehyde, **1c**; 2-bromobenzaldehyde, **1d**; 4-methoxybenzaldehyde, **1e**; 2-pyridinecarboxaldehyde, **1f**; 3-pyridinecarboxaldehyde, **1g**; 4-pyridinecarboxaldehyde, **1h**) as starting materials were dissolved in anhydrous ethanol, acetic acid was added dropwise to the solution as a catalyst. And then, hydrazine (**2a**), ethylenediamine (**2b**), diethylenetriamine (**2c**), and *N*,*N*-di(2-aminoethyl)ethylenediamine (**2d**), respectively, was added to the mixture under reflux for 2~6 h. Finally, the target compounds **3a-f**, **4a-g**, **5a-b**, and **6a-b** were obtained by crystallization, and the derivatives were characterized by ^{1}H NMR, ^{13}C NMR, and IR.

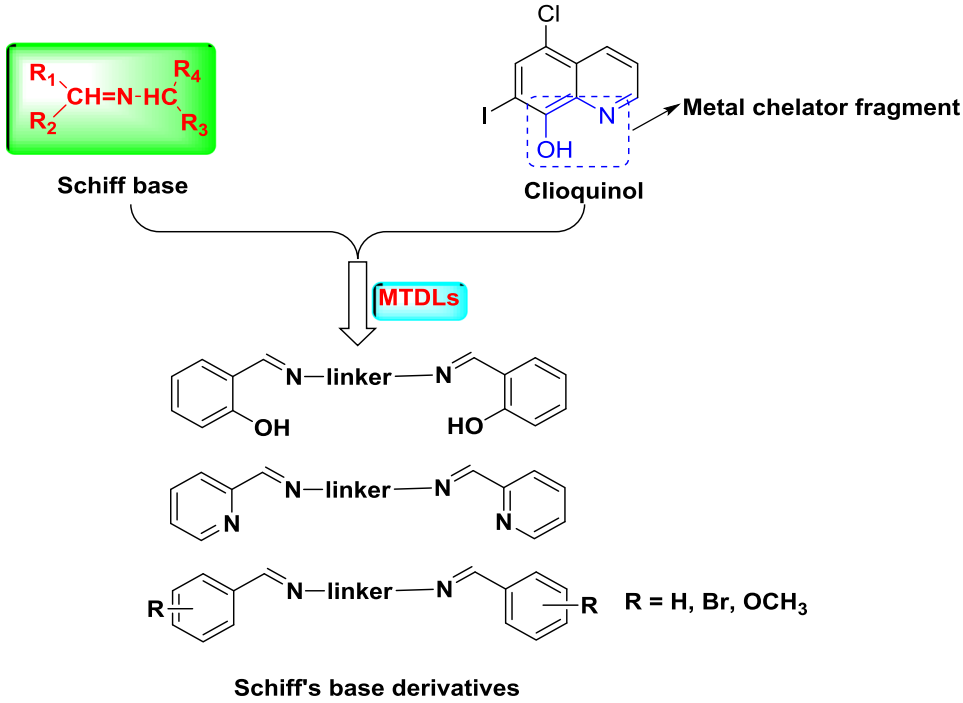

Fig. 1 The design strategy of Schiff's base derivatives

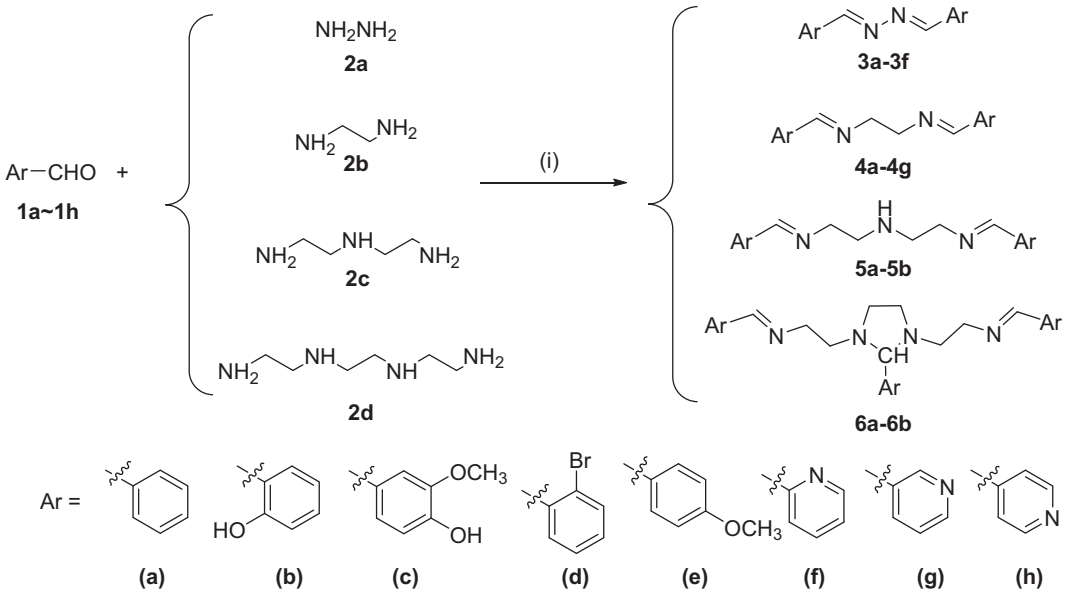

Scheme 1 Synthesis of target compounds **3a-f**, **4a-g**, **5a-b**, and **6a-b**. Reagents and conditions: (i) ArCHO(**1a~1h**), anhydrous ethanol, reflux, 2–6 h

Biological activity

Inhibition of monoamine oxidases

All the synthesized Schiff's base derivatives were evaluated for their inhibitory activity against human MAO-A and MAO-B by a fluorimetric method [19]. Rasagiline was used as the positive control. The results were summarized in Table 1, most of these derivatives showed much better MAO-B inhibitory activities than towards MAO-A, indicating that these compounds were selective MAO-B inhibitors. Generally, the primary amine skeleton and the aromatic formaldehyde significantly influenced the MAO-B inhibitory activity. When the primary amine skeleton was hydrazine, the target compounds **3a-f** exhibited better inhibitory activity of MAO-B than other derivatives

Table 1 In vitro IC_{50} values of test compounds toward *h*MAO-A, *h*MAO-B and inhibition of self-/Cu^{2+}-induced A$\beta_{1\text{-}42}$ aggregation

Compd	Ar	IC_{50} (μM)[a]		ORAC[d]	% inhibition of Aβ$_{1\text{-}42}$ aggregation[e]	
		MAO-A(%)[b]	MAO-B		Self-induced[f]	Cu^{2+}-induced[g]
3a		18.5 ± 0.67	30.6 ± 0.87	0.4 ± 0.01	23.5 ± 1.7	—
3b		23.1 ± 0.69	0.0084 ± 0.0006	2.3 ± 0.05	31.8 ± 1.3	62.3 ± 2.89
3c		33.3 ± 2.6	28.9 ± 1.6	2.6 ± 0.08	46.2 ± 2.3	—
3d		36.9 ± 1.3	14.0 ± 0.48	0.6 ± 0.03	24.3 ± 1.5	—
3e		12.4 ± 0.79	15.4 ± 0.59	0.5 ± 0.02	20.1 ± 1.3	—
3f		16.4 ± 1.1	34.2 ± 0.93	0.5 ± 0.03	14.5 ± 0.69	—
4a		6.5 ± 0.37	30.4 ± 2.1	0.3 ± 0.02	20.9 ± 1.1	—
4b		0.3 ± 0.12	n.a.[c]	2.5 ± 0.08	37.8 ± 2.5	—
4c		13.0 ± 0.47	n.a.[c]	2.7 ± 0.07	28.9 ± 2.1	—
4d		7.3 ± 0.66	n.a.[c]	0.3 ± 0.02	16.5 ± 0.92	—
4e		5.6 ± 0.38	54.6 ± 2.6	0.6 ± 0.03	21.1 ± 1.2	—
4f		0.4 ± 0.01	11.9 ± 0.41	0.6 ± 0.01	21.4 ± 0.68	—
4g		2.4 ± 0.39	53.5 ± 2.6	0.5 ± 0.05	28.6 ± 0.89	—
5a		27.5 ± 1.7	n.a.[c]	2.7 ± 0.09	13.1 ± 0.78	—
5b		13.8 ± 0.86	55.7 ± 3.7	2.8 ± 0.07	13.2 ± 1.1	—
6a		12.2 ± 0.63	n.a.[c]	2.9 ± 0.06	20.6 ± 0.88	—
6b		3.6 ± 0.14	n.a.[c]	2.7 ± 0.08	24.1 ± 1.3	—
rasagiline		0.59 ± 0.04 μM	0.029 ± 0.003	—	—	—
curcumin		—	—		38.1 ± 2.6	67.4 ± 4.16

[a]IC_{50}: 50% inhibitory concentration(means SD of three experiments)

[b]Results are expressed as μM of Trolox equivalent/μM of tested compound

[c]For inhibition of Aβ aggregation, the thioflavin-T fluorescence method was used, data are presented as the mean ± SEM of three independent experiments

[d]MAO-A inhibition rate at the test concentration of 12.5 μM

[e]Inhibition of self-induced A$\beta_{1\text{-}42}$ aggregation, the concentration of tested compounds and A$\beta_{1\text{-}42}$ were 25 μM

[f]Inhibition of Cu^{2+}-induced A$\beta_{1\text{-}42}$ aggregation produced by tested compounds at 25 μM

[g]n.a. = no active. Compounds defined "no active" means that inhibition is less than 5.0% at a concentration of 50 μM in the assay condition

(Table 1), particularly, compound **3b** showed the best potency for inhibition of MAO-B with an IC_{50} value of 8.4 nM, which was better than the reference compound rasagiline (IC_{50} = 29 nM), and the selective index toward MAO-B of **3b** was higher than rasagiline. In addition, the structure-activity-relationship also displayed that benzaldehyde fragment (**3a**) showed moderate MAO-B inhibitory activity (IC_{50} = 30.6 μM), when replacing benzaldehyde fragment with salicylaldehyde fragment to get compound **3b**, the MAO-B inhibitory activity sharply increased to 8.4 nM, maybe the 2-hydroxy moiety of salicylaldehyde served as a critical role in MAO-B inhibitory potency. When replacing benzaldehyde fragment of **3a** with 4-hydroxy-3-methoxybenzaldehydes fragment to get compound **3c**, the MAO-B inhibitory activity did not show obvious change. Subsequently, when replacing benzaldehyde fragment of **3a** with 2-pyridinecarboxaldehyde, 3-pyridinecarboxaldehyde, and 4-pyridinecarboxaldehyde, respectively, to obtain compounds **3d**, **3e**, and **3f**, respectively, the IC_{50} values of MAO-B inhibitory activities were 14.0 μM, 15.4 μM and 34.2 μM, respectively, indicating that the 2-pyridinecarboxaldehyde

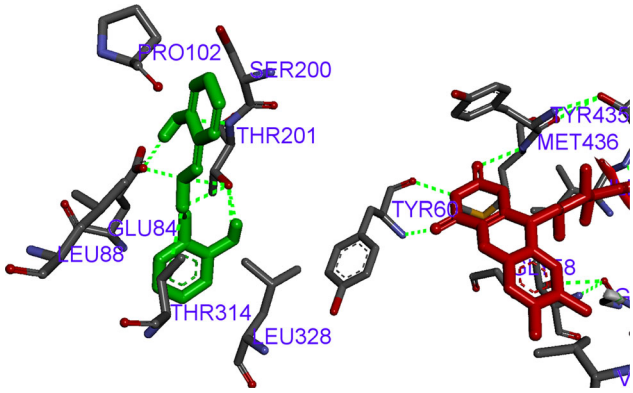

Fig. 2 Compound **3b** (green stick) interacting with residues in the binding site of *hu*MAO-B (PDB code: 2V60)

and 3-pyridinecarboxaldehydefragment would be beneficial for the MAO-B inhibition. Furthermore, the MAO-B inhibitory activity significantly decreased as the length of linker increased, such as **3b** < **4b**, **5a**, and **6a**; **3c** < **4c**, **5b**, and **6b**, implying that the the more long linker was harmful to the MAO-B inhibitory potency. In short, compound **3b** presented the best selective MAO-B inhibitory potency and was worth in-depth study.

Molecular modeling study of MAO-B

To further explore the binding mode of **3b** with MAO-B, a molecular docking was performed with the X-ray crystal structures of human MAO-B (PDB code: 2V60) [20]. In **3b**-MAO-B complex (Fig. 2), the O atom of hydroxyl group in one side of **3b** interacted with key amino acid Thr 201 via one intermolecular hydrogen bonding, the H atom of hydroxyl group in one side of **3b** formed one intermolecular hydrogen bonding with key amino acid Glu84, and the H atom of hydroxyl group interacted with N atom of **3b** via intramolecular hydrogen bonding interaction. Moreover, the hydroxyl group in another side of 3b interacted with key amino acid Thr201 via two intermolecular hydrogen bonding interactions. Meanwhile, the N atom in one side of **3b** interacted with key amino acid Thr201 via one intermolecular hydrogen bonding, and the N atom in another side of **3b** interacted with key amino acid Thr201 and Thr314 via two intermolecular hydrogen bonding interactions. Besides, there were some hydrophobic interactions could be observed between the ligand **3b** and amino acids Pro102, Leu88, and Leu328 in MAO-B. Thus, the observed interactions provided rational explanation for the high MAO-B inhibitory activity toward **3b**.

Antioxidant activity assay

The antioxidant activity of target compounds were evaluated by oxygen radical absorbance capacity fluorescein (ORAC-FL) method using Trolox (vitamin E analog) as a referenced compound [21]. As displayed in Table 1, all the target compounds displayed moderate to good antioxidant potency with ORAC value of 0.3–2.9 *eq*. Generally speaking, the derivatives (**3b**, **3c**, **4b**, **4c**, **5a**, **5b**, **6a**, **6b**) with hydroxyl group showed better antioxidant activity than other groups, revealing that the hydroxyl group of target compounds was crucial to the radical scavenging capability and could contribute to the antioxidant activities. Moreover, the data showed that other benzaldehyde fragment without hydroxyl group did not show significant influence on the antioxidant activity.

Inhibition of self-induced $A\beta_{1-42}$ aggregation

All the target compounds were selected to test the self-induced $A\beta_{1-42}$ aggregation inhibitory activity by thioflavin T (ThT) fluorescence assay using curcumin as reference compound [22]. According to the results in Table 1, all the derivatives showed moderate to good inhibitory potency towards self-induced $A\beta_{1-42}$ aggregation compared with curcumin (38.1%). Among these derivatives, compound **3c** (46.2%) showed the best inhibitory potency against self-induced $A\beta_{1-42}$ aggregation, which was better than curcumin. Moreover, the length of linker and the aromatic formaldehyde remarkably influenced the inhibitory activity, generally, the inhibition rate declined as the length of linker increased. In addition, the electron-donating group (such as OH group) indicated better inhibition rate than other groups, such as compounds **3b**, **3c**, **4b**, and **4c**. Especially, compound **3b** displayed good inhibition rate with 31.8%, which was similar with curcumin.

Metal-chelating properties of 3b

The UV-visual spectrometry was applied to test the chelation ability of compound **3b** using Cu^{2+}, Fe^{2+}, Zn^{2+} and Al^{3+} [21, 22]. As presented in Fig. 3, when adding Cu^{2+}, the characteristic peak of **3b** presented a red shift from 354 nm to 398 nm, while, when treating with Fe^{2+}, Zn^{2+}, and Al^{3+}, respectively, the electronic spectra did not show obvious shift, revealing that compound **3b** was a selective metal chelator. Furthermore, the molar ratio method was employed to assess the stoichiometry of the **3b**-Cu^{2+} complex at 398 nm. As exhibited in Fig. 4, the two straight lines intersected at a mole fraction of 1.98, displaying a 1:2 stoichiometry for the **3b**-Cu^{2+} complex.

Effects on Cu^{2+}-induced $A\beta_{1-42}$ aggregation

According to the above data, compound **3b** was a selective Cu^{2+} chelator, in order to further assess the inhibition effect of **3b** on Cu^{2+}-induced $A\beta_{1-42}$ aggregation, ThT binding

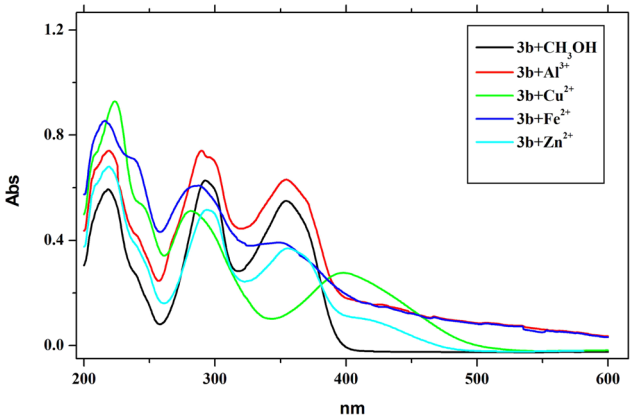

Fig. 3 The UV spectrum of compound **3b** (37.5 μM, in methanol) alone or in the presence of $CuCl_2$, $FeSO_4$, $ZnCl_2$. and $AlCl_3$ (37.5 μM, in methanol)

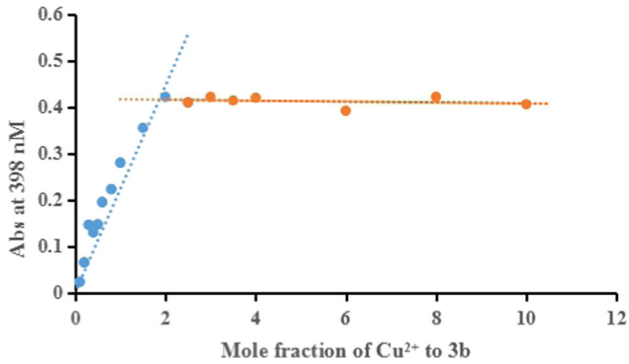

Fig. 4 Determination of the stoichiometry of complex-Cu^{2+} by using molar ratio method through titrating the methanol solution of compound **3d** with ascending amounts of $CuCl_2$. The final concentration of tested compound was 37.5 μM, and the final concentration of Cu^{2+} ranged from 3.75 to 375 μM

assay was performed [22]. The result from Table 1 showed that compound **3b** significantly inhibit Cu^{2+}-induced A$\beta_{1\text{-}42}$ aggregation (62.3%), which was similar with the positive compound curcumin (67.4%). Moreover, transmission electron microscopy (Fig. 5) was used to observe the Cu^{2+}-induced A$\beta_{1\text{-}42}$ aggregation experiments, which was consistent with the ThT assay.

Neuroprotective effects on H_2O_2-induced PC12 cell injury

Compounds **3b, 3c**, and **4b** were selected to test the neuroprotective effects against H_2O_2-induced PC12 cell injury by 3-(4,5-dimethylthiazol-2-yl)-2,5-diphenyltetrazolium (MTT) assays and lactate dehydrogenase (LDH) assay using Vitamine E (VE) as the positive compound [21]. As displayed in Fig. 6a, when PC12 cells were treated with 100 μM H_2O_2, the cell viability sharply decreased to 57.8% ($p < 0.01$) compared with the normal group. When treating with 100 μM VE, the cell viability increased to 67.7%. Under the same experiments condition, when treating with 10 μM compounds **3b, 3c**, and **4b**, the cell viabilities increased to 74.3, 69.4, and 81.8%, respectively. When the concentration increased to 100 μM, the cell viabilities were 79.1, 60.9, and 84.3%, respectively. Therefore, the data showed that compounds **3b, 3c** and **4b** showed better neuroprotective effect than VE. In addition, neuroprotective effect of compounds **3b, 3c**, and **4b** were also evaluated through LDH assay [21]. As displayed in Fig. 6b, 100 μM H_2O_2 was exposed to the PC12 cell, the LDH vitality suddenly increased to 785.5 ($p < 0.01$) compared with normal group (674.7), when treating with 100 μM VE, the LDH vitality decreased to 693.1. When treating with 10 μM compounds **3b**, **3c**, and **4b**, the LDH vitality declined to 590.4, 579.6 and 724.1, respectively. When the concentration increased to 100 μM, the vitality were 570.6, 659.8, and 681.3. In summary, the data reveled that compounds **3b**, **3c**, and **4b** displayed potential protective effect against H_2O_2-induced PC12 cell injury.

In vitro blood-brain barrier permeation assay

The parallel artificial membrane permeation assay (PAMPA) of the blood-brain barrier was applied to evaluate the BBB permeability of **3b** [23, 24]. 11 commercial drugs were selected to validate the assay (Table S1), $P_e(\text{exp}) = 0.9163P_e(\text{bibl.}) - 0.2247$ ($R^2 = 0.9558$) (Fig. S1), was obtained by experimental data versus the reported values. We determined that compounds with permeability above 3.44×10^{-6} cm/s could cross the blood-brain barrier based on the limit established by Di et al. (Table S2). The measured data were shown in Table 2, compound **3b** showed 13.29×10^{-6} cm/s permeability, indicating good BBB permeability in vitro.

Theoretical evaluation of ADME properties

The druglike properties of **3b** were evaluated using Molinspiration property program, the items including log *P*, topological polar surface area (TPSA), the number of hydrogen-bond acceptors, and the number of hydrogen-bond donors [25]. As presented in Tables 3, 3b complied with the Lipinski's rule of five, which could be a potent candidate for the treatment of AD.

Conclusion

In summary, a series of Schiff's base derivatives was rationally designed and synthesized, the biological activity of these derivatives were evaluated by MAO-A/MAO-B inhibition, antioxidant activity, A$\beta_{1\text{-}42}$ aggregation effects, metal chelation property and neuroprotective effect.

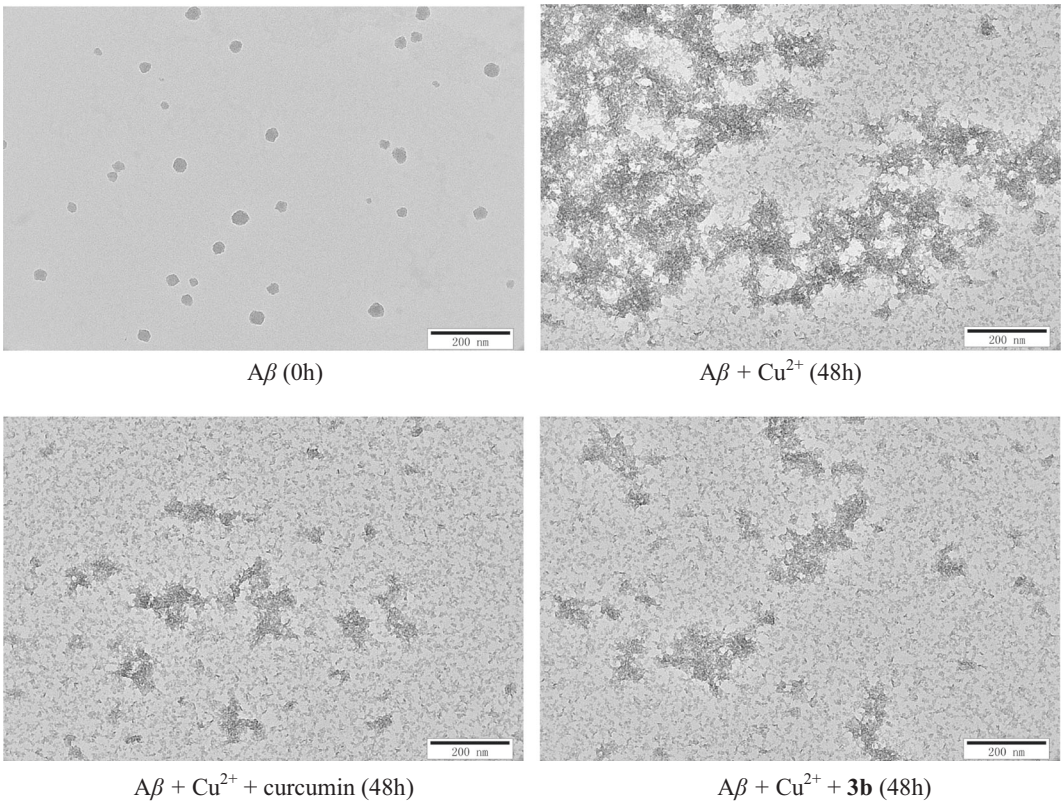

Fig. 5 TEM images of Aβ species from inhibition experiments

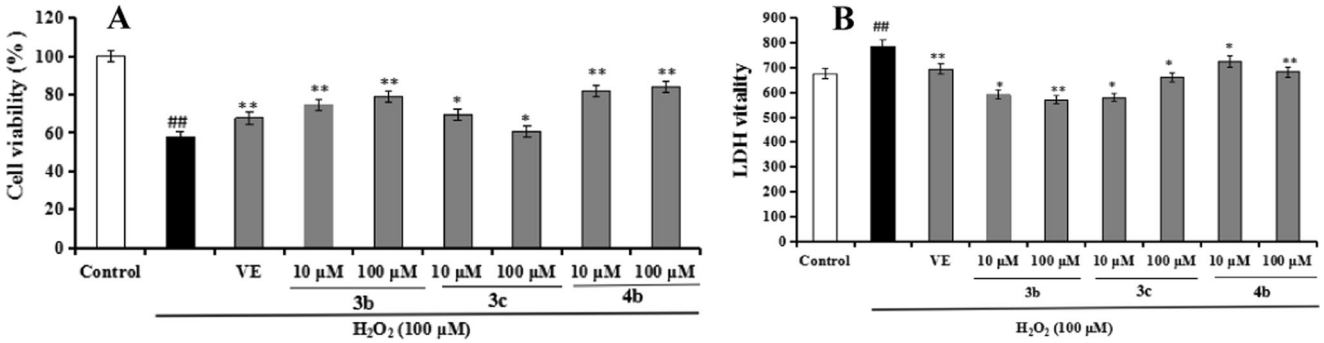

Fig. 6 **a** The cell viability (%) of compounds **3b, 3c**, and **4b** on H_2O_2-induced PC12 cell injury by MTT assay. **b** The LDH vitality of compounds **3b, 3c**, and **4b** on H_2O_2-induced PC12 cell injury. Three independent experiments were carried out in triplicate. Data were expressed as mean ± SD and percentage of control value. ##$p < 0.01$ vs control; **$p < 0.01$, *$p < 0.05$ vs H_2O_2 group

Table 2 Permeability Pe ($\times 10^{-6}$ cm/s) of compound **3b** and its predictive penetration in the CNS

Compound[a]	Pe ($\times 10^{-6}$ cm/s)[b]	Prediction
3b	13.29 ± 1.23	CNS+

[a]Compound **3b** was dissolved in DMSO at 5 mg/mL and diluted with PBS/EtOH (70:30). The final concentration of compounds was 100 μg/mL

[b]Values are expressed as the mean ± SD of three independent experiments

The results revealed that compound **3b** showed the best MAO-B inhibitory activity with IC_{50} value of 8.4 nM, which was confirmed by the docking study. Compound **3b** also displayed significant antioxidant activity (ORAC = 2.3 eq) and remarkably inhibited self-induced $A\beta_{1\text{-}42}$ aggregation with 31.8% inhibition rate. In addition, compound **3b** was a metal chelator and could inhibit Cu^{2+}-induced $A\beta_{1\text{-}42}$ aggregation (62.3%). Moreover, compound **3b** showed good neuroprotective effects on H_2O_2-induced PC12 cell injury. Further, compound **3b** could cross BBB in vitro and

Table 3 Theoretical prediction of the ADME properties of compound **3b**

Comp.[a]	Log *P*	MW	TPSA (Å^2)	n-ON	n-OHNH	nviolations	nrotb	Volume (Å^3)
Lipinski's rule of five	≤ 5	≤ 500		≤ 10	≤ 5		≤ 10	
3b	3.09	240.26	65.18	4	2	0	3	218.01

MW molecular weight, *TPSA* topological polar surface area, *n-ON* number of hydrogen acceptors, *n-OHNH* number of hydrogen bond donors

[a]The data were determined with the Molinspiration calculation software

exhibited good drug-like properties. Therefore, compound **3b** could be a promising multifunctional agent for the treatment of AD. Further studies to evaluate compound **3b** in vivo and to develop structural refinements are in progress and will be reported in due course.

Experimental

Chemistry

General information

All materials were obtained from commercial sources and utilized without further purification unless otherwise indicated. Melting points were measured on X-5 precision micro melting point apparatus (China). ^{1}H NMR (400 MHz) and ^{13}C NMR (100 MHz) spectra were recorded on a Varian INOVA spectrometer and referenced to Tetramethylsilane (TMS), using $CDCl_3$ or DMSO-d_6 as solvents. Chemical shifts (δ) are reported in ppm. Splitting patterns are designated as s, single; d, doublet; dd, double-doublet; t, triplet; m, multiplet. MS spectra data were obtained on an Agilent-6210 TOF LC-MS spectrometer.

General procedure for the preparation of Schiff's base derivatives 3a-f, 4a-g, 5a-b, and 6a-b

The excessive amounts of benzaldehyde derivatives **1a~h** (2-3 mmol) were dissolved in anhydrous ethanol (8 mL), acetic acid was added two or three drops to the solution as a catalyst. Finally, hydrazine (**2a**), ethylenediamine (**2b**), diethylenetriamine (**2c**), or triethylenetetramine (**2d**) (1 mmol) was added to the aforementioned solution, respectively. The reaction mixture was stirred under reflux condition for 6 h monitored by TLC. After reaction finished, the solvent was concentrated under reduced pressure. The crude product was purified by crystallization from anhydrous ethanol to give the target compounds **3a-f**, **4a-g**, **5a-b**, and **6a-b**.

1,2-di((E)-benzylidene)hydrazine (3a) Bright yellow solid, 65.71% yield, mp: 94.2–94.8 °C, 98.7% purity. ^{1}H NMR (400 MHz, $CDCl_3$) δ 8.68 (s, 2H, 2 × =CH), 7.86 (d, J = 2.0 Hz, 2H), 7.84 (d, J = 8.4 Hz, 2H), 7.46 (d, J = 2.0 Hz, 4H), 7.45 (d, J = 1.6 Hz, 2H). ^{13}C NMR (100 MHz, DMSO-d_6): 161.9, 134.3, 131.8, 129.4, 128.8. IR (KBr, cm^{-1}) 1622.2 (C=N), 1574.0, 1488.6, 1445.8. MS (ESI) m/z: 209.1 [M+H] $^+$.

2,2′-((1E,1′E)-hydrazine-1,2-diylidenebis(methanylylidene)) diphenol (3b) Bright yellow solid, 71.08% yield, mp: 196.4–197.2 °C, 99.0% purity. ^{1}H NMR (400 MHz, $CDCl_3$) δ 11.40 (s, 2H), 8.72 (s, 2H), 7.40–7.35 (m, 4H), 7.04 (d, J = 8.4 Hz, 2H), 6.98 (t, J = 7.6 Hz, 2H).^{13}C NMR (100 MHz, DMSO-d_6): 163.3, 159.1, 133.7, 131.3, 120.1, 118.7, 117.0. IR (KBr, cm^{-1}) 3434.6(O-H), 1624.1(C=N), 1573.6, 1487.1, 1387.6. MS (ESI) m/z: 241.1 [M+H] $^+$.

4,4′-((1E,1′E)-hydrazine-1,2-diylidenebis(methanylylidene)) bis(2-methoxyphenol) (3c) Light yellow solid, 73.63% yield, mp 178.4–179.6 °C, 98.6% purity. ^{1}H NMR (400 MHz, $CDCl_3$) δ 8.58 (s, 2H), 7.54 (d, J = 1.6 Hz, 2H), 7.21 (dd, J_1 = 6.4 Hz, J_2 = 1.6 Hz, 2H), 6.97 (d, J = 8.4 Hz, 2H), 5.99 (s, 2H), 3.99 (s, 6H). ^{13}C NMR (100 MHz, DMSO-d_6): 161.1, 150.4, 148.5, 126.0, 123.9, 115.0, 110.6, 56.0. IR (KBr, cm^{-1}) 3480.4 (O-H), 2933.5 (C-H), 1623.9 (C=N), 1600.6, 1540.0, 1459.0. MS (ESI) m/z: 301.1 [M+H]$^+$.

(1E,2E)-1,2-bis(pyridin-2-ylmethylene)hydrazine (3d) Yellow solid, 74.38% yield, mp 172.4–173.6 °C, 98.6% purity. ^{1}H NMR (400 MHz, $CDCl_3$) δ9.03 (s, 2 H, 2 × =CH), 8.21–7.26 (m, 8H, 2 × C_6H_4). IR (KBr, cm^{-1}) 1611.2 (C=N), 1586.1, 1554.5, 1463.1, 1434.3. MS (ESI) m/z: 211.1 [M+H]$^+$.

(1E,2E)-1,2-bis(pyridin-3-ylmethylene)hydrazine (3e) Yellow solid, 75.38% yield, mp 145.5–146.6 °C, 98.4% purity. ^{1}H NMR (400 MHz, $CDCl_3$) δ 8.74 (dd, J_1 = 4.0 Hz, J_2 = 0.8 Hz, 2H), 8.70 (s, 2H), 8.13 (d, J = 8.0 Hz, 2H), 7.81 (dt, J_1 = 7.6 Hz, J_2 = 1.2 Hz, 2H), 7.39 (dd, J_1 = 4.0 Hz, J_2 = 0.8 Hz, 1H), 7.37 (dd, J_1 = 4.0 Hz, J_2 = 0.8 Hz, 1H). ^{13}C NMR (100 MHz, DMSO-d_6): 161.6, 152.6, 150.4, 137.6, 126.2, 122.2. IR (KBr, cm^{-1}) 1628.9 (C=N), 1583.0, 1463.4, 1437.5. MS (ESI) m/z: 211.1 [M+H]$^+$.

(1E,2E)-1,2-bis(pyridin-4-ylmethylene)hydrazine (3f) Yellow solid, 61.35% yield, mp 145.7–146.0 °C, 98.7% purity. ^{1}H NMR (400 MHz, $CDCl_3$) δ 8.99 (s, 2 H), 8.71 (d, J = 8.0 Hz, 2H), 8.69 (s, 2H), 8.23 (d, J = 8.0 Hz, 2H), 7.43 (d,

$J = 4.8$ Hz, 1H), 7.41 (d, $J = 4.8$ Hz, 1H). ^{13}C NMR (100 MHz, DMSO-d_6): 160.1, 152.5, 150.4, 135.3, 129.9, 124.6. IR (KBr, cm^{-1}) 1627.1 (C=N), 1582.8, 1470.2, 1418.0. MS (ESI) m/z: 211.1 $[M+H]^+$.

(1E,1′E)-N,N′-(ethane-1,2-diyl)bis(1-phenylmethanimine) (4a) Bright yellow solid, 77.46% yield, mp 180.4–182.4 °C, 98.6% purity. ^1H NMR (400 MHz, $CDCl_3$) δ 8.76 (dd, $J_1 = 3.6$ Hz, $J_2 = 1.2$ Hz, 4H), 8.58 (s, 2H), 7.71 (dd, $J_1 = 3.2$ Hz, $J_2 = 1.2$ Hz, 4H). ^{13}C NMR (100 MHz, DMSO-d_6): 160.1, 151.0, 140.9, 122.5. IR (KBr, cm^{-1}) 1627.5 (C=N), 1594.5, 1551.7, 1417.5. MS (ESI) m/z: 237.1 $[M+H]^+$.

2,2′-((1E,1′E)-(ethane-1,2-diylbis(azanylylidene))bis(methanylylidene))diphenol (4b) Bright yellow solid, 70.4% yield, 98.3% purity. ^1H NMR (400 MHz, $CDCl_3$) δ 8.29 (s, 2H, 2 =CH), 7.70–7.68 (m, 4H, C_6H_5), 7.40–7.36 (m, 4H, C_6H_5), 3.98 (s, 4H, $2 \times CH_2$). ^{13}C NMR (100 MHz, DMSO-d_6): 161.6, 129.9, 129.4, 114.5, 61.5, 55.7. MS (ESI) m/z: 269.1 $[M+H]^+$.

4,4′-((1E,1′E)-(ethane-1,2-diylbis(azanylylidene))bis(methanylylidene))bis(2-methoxyphenol) (4c) Bright yellow solid, 68.8% yield, mp 124.5–125.0 °C, 97.8% purity. ^1H NMR (400 MHz, $CDCl_3$)δ 13.23 (s, 2H, $2 \times OH$), 8.36 (s, 2H, $2 \times CH =$), 7.23–7.30 (m, 4H, C_6H_4), 6.86–6.95 (m, 4H, C_6H_4), 3.94 (s, 4H, $2 \times CH_2$). ^{13}C NMR (100 MHz, DMSO-d_6): 167.4, 161.0, 132.8, 132.1, 119.1, 119.0, 116.9, 59.2. IR (KBr, cm^{-1}) 3438 (O-H), 2928 (C-H), 1634 (C=N), 1578, 1497, 1459, 1416, 1284 (C-N), 1202, 1194 (C-O-C). MS (ESI) m/z: 329.1 $[M+H]^+$.

(1E,1′E)-N,N′-(ethane-1,2-diyl)bis(1-(2-bromophenyl)methanimine) (4d) Bright yellow solid, 60.21% yield, 98.0% purity. ^1H NMR (400 MHz, DMSO) δ 9.54 (s, 2H, $2 \times OH$), 8.19 (s, 2H, $2 \times CH =$), 7.32–6.70 (m, 6H, $2 \times C_6H_3$), 3.78 (s, 10H, $2 \times CH_2 + 2 \times OCH_3$). ^{13}C NMR (100 MHz, DMSO-d_6): 161.9, 148.3, 128.4, 128.4, 123.1, 115.7, 110.40, 61.4, 55.9. MS (ESI) m/z: 393.0 $[M+H]^+$.

(1E,1′E)-N,N′-(ethane-1,2-diyl)bis(1-(4-methoxyphenyl) methanimine) (4e) Bright yellow solid, 56.27% yield, 98.3% purity. ^1H NMR (400 MHz, $CDCl_3$) δ 8.65 (s, 2H, $2 \times CH =$), 8.0–7.23 (m, 8H, $2 \times C_6H_4$), 4.03(s, 4H, $2 \times CH_2$). ^{13}C NMR (100 MHz, DMSO-d_6): 161.1, 134.5, 133.5, 132.9, 129.0, 128.4, 124.6, 60.9. MS (ESI) m/z: 297.2 $[M+H]^+$.

(1E,1′E)-N,N′-(ethane-1,2-diyl)bis(1-(pyridin-2-yl)methanimine) (4f) Yellow solid, 62% yield, mp 153.2–153.5 °C, 98.5% purity. ^1H NMR (400 MHz, $CDCl_3$)δ 8.20 (s, 2H, $2 \times CH =$), 7.64–7.62 (m, 4H, C_6H_4), 6.90–6.88 (m, 4H, C_6H_4), 3.91 (t, 4H, $2 \times CH_2$), 3.81 (s, 6H, $2 \times OCH_3$). IR (KBr, cm^{-1}) 3440 (O-H), 2969, 2919 (C-H), 1641(C=N), 1604, 1509, 1457, 1308 (C-N), 1282, 1020 (C-O-C). 239.1 $[M+H]^+$.

(1E,1′E)-N,N′-(ethane-1,2-diyl)bis(1-(pyridin-4-yl)methanimine) (4g) Yellow solid, 49.6% yield, 98.7% purity. ^1H NMR (400 MHz, $CDCl_3$) δ 8.62 (s, 2H, $2 \times CH =$), 8.42–7.29 (m, 8H, $2 \times C_6H_4$), 4.06(s, 4H, $2 \times CH_2$). ^{13}C NMR (100 MHz, DMSO-d_6): 163.5, 154.5, 149.8, 137.3, 125.5, 120.9. MS (ESI) m/z: 239.1 $[M+H]^+$.

2,2′-((1E,1′E)-((azanediylbis(ethane-2,1-diyl))bis(azanylylidene))bis(methanylylidene))diphenol (5a) Yellow solid, 40.3% yield, 97.6% purity. ^1H NMR (400 MHz, $CDCl_3$) δ 8.83(s, 2 H, $2 \times CH =$), 8.64–7.33 (m, 8H, $2 \times C_6H_4$), 4.02 (s, 4H, $2 \times CH_2$). MS (ESI) m/z: 312.2 $[M+H]^+$.

4,4′-((1E,1′E)-((azanediylbis(ethane-2,1-diyl))bis(azanylylidene))bis(methanylylidene))bis(2-methoxyphenol) (5b) Yellow solid, 36.8% yield, 97.8% purity. ^1H NMR (400 MHz, $CDCl_3$) δ 8.67–8.69 (m, 4H, $2 \times CH = + C_6H_4$), 8.29 (t, 2H, C_6H_4), 7.58–7.55 (m, 4H, C_6H_4), 4.06 (q, 4H, $2 \times CH_2$). ^{13}C NMR (100 MHz, DMSO-d_6): 161.4, 150.8, 143.0, 122.2, 61.0. MS (ESI) m/z: 372.2 $[M+H]^+$.

2,2′-((1E,1′E)-(((2-(2-hydroxyphenyl)imidazolidine-1,3-diyl) bis(ethane-2,1-diyl))bis(azanylylidene))bis(methanylylidene))diphenol (6a) Bright yellow solid, 33.02% yield, 97.6% purity. ^1H NMR (400 MHz, $CDCl_3$) δ 13.12–13.27 (m, 1H, OH), 8.25 (s, 1H, CH =), 6.79–7.31 (m, 9H, $2 \times C_6H_4$, CH =), 3.42–3.83 (m, 5H, $2 \times CH_2$+OH), 2.95~2.98 (m, 1H, NH), 2.66–2.69 (m, 4H, $2 \times CH_2$). IR (KBr, cm^{-1}) 3427(O-H), 2860, 2822(C-H), 1631(-CH=N), 1580, 1495, 1456, 1414.9, 1261(C-N), 1206, 1116 (C-O-C). MS (ESI) m/z: 459.2 $[M+H]^+$.

4,4′-((1E,1′E)-(((2-(4-hydroxy-3-methoxyphenyl)imidazolidine-1,3-diyl)bis(ethane-2,1-diyl))bis(azanylylidene))bis (methanylylidene))bis(2-methoxyphenol) (6b) Yellow solid, 68.48% yield, mp 103.2–104.0 °C, 97.7% purity. ^1H NMR (400 MHz, $CDCl_3$) δ 13.24 (s, 2H), 10.70 (s, 1H), 8.25 (s, 2H), 7.29 (dt, $J_1 = 6.8$ Hz, $J_2 = 2.0$ Hz, 2H), 7.25 (dd, $J_1 = 6.4$ Hz, $J_2 = 0.8$ Hz, 1H), 7.21 (dd, $J_1 = 6.0$ Hz, $J_2 = 1.6$ Hz, 2H), 7.00 (dd, $J_1 = 6.0$ Hz, $J_2 = 1.6$ Hz, 1H), 6.93 (d, $J = 8.0$ Hz, 2H), 6.86 (dt, $J_1 = 6.8$ Hz, $J_2 = 0.8$ Hz, 2H), 6.82 (dd, $J_1 = 3.6$ Hz, $J_2 = 0.8$ Hz, 1H), 6.82 (dd, $J_1 = 3.6$ Hz, $J_2 = 0.8$ Hz, 1H), 6.80 (dd, $J_1 = 4.4$ Hz, $J_2 = 0.8$ Hz, 1H), 3.83 (s, 1H), 3.60 (t, $J = 6.4$ Hz, 4H), 3.45–3.41 (m, 2H), 2.99 (t, $J = 6.4$ Hz, 1H), 2.95 (t, $J = 6.4$ Hz, 1H), 2.71–2.62 (m, 4H). IR (KBr, cm^{-1}) 3439 (O-H), 2856、2802 (C-H), 1632 (C=N), 1581, 1494, 1460, 1415, 1372, 1312(C-N), 1206, 1033 (C-O-C). MS (ESI) m/z: 549.3 $[M+H]^+$.

Biological activity

Human MAO-A and MAO-B inhibition studies

Recombinant human MAO-A and -B were purchased from Sigma-Aldrich, all the test compounds were prepared in DMSO (2.5 mM) and diluted with potassium phosphate buffer (100 mM, pH 7.40, containing KCl 20.2 mM). Rasagiline was used as the positive compound. Kynuramine was used as MAOs substrate and the final concentration was 45 μM for MAO-A and 30 μM for MAO-B. The detailed procedure referenced our previous work [19, 20].

Molecular modeling studies

Docking was employed to identify the potential binding of compound **3b** to MAO-B. The crystal structure of *hu*MAO-B (PDB code: 2V60) was obtained from the Protein Data Bank after removing the original inhibitors and water molecules [19, 20]. The 3D Structure of **3b** was built and performed geometry optimization by molecular mechanics. Docking studies were performed using the AUTODOCK 4.2.6 program and each docked system was performed by 100 runs of the AUTODOCK search by the Lamarckian genetic algorithm. A cluster analysis was performed on the docking results using a root mean square tolerance of 1.0 and the lowest energy conformation of the highest populated cluster was selected for analysis. Graphic manipulations and visualizations were done by Autodock Tools or Discovery Studio 2.5 software [19, 20].

Antioxidant activity assay

The ORAC-FL method was used to test the antioxidant activity. The procedure referenced our previous work [21, 22].

Metal binding studies

To investigate the metal binding ability of compound, the UV absorption of the tested compound **3b**, in the absence or presence of $CuCl_2$, $FeSO_4$, $ZnCl_2$, and $AlCl_3$, were carried out in a Shimadzu UV-2450 spectrophotometer, and recorded with wavelength ranging from 200 to 600 nm. The molar ration method was performed to determine the stoichiometry of the complex compound-metal by titrating the methanol solution of tested compound with ascending of $CuCl_2$. The procedure referenced our previous work [21, 22].

Self-/Cu^{2+}-induced $A\beta_{1\text{-}42}$ aggregation inhibition

To study self-/Cu^{2+}-induced $A\beta_{1\text{-}42}$ aggregation inhibition, a thioflavin T-based fluorometric assay was performed. The procedure referenced our previous work [21, 22].

In vitro blood-brain barrier permeation assay

The blood-brain barrier penetration of compounds was evaluated using the PAMPA [23, 24]. Commercial drugs were purchased from Sigma and Alfa Aesar. Porcine brain lipid was obtained from Avanti Polar Lipids. The donor microplate (PVDF membrane, pore size 0.45 mm) and acceptor microplate were both from Millipore. The 96-well UV plate (COSTAR) was from Corning Incorporated. According to the detailed procedure in our previous work, we concluded that compounds with P_e values above 3.44×10^{-6} cm/s could cross the blood-brain barrier.

Acknowledgements This work was supported by funding from the China Scholarship Council (NO.201808410456). International Training of High-level Talents in Henan Province in 2019 (NO.17) (Henan Foreign Experts Bureau), the Key Scientific Research Project of Colleges and Universities in Henan Province (NO.20A350006), and the Special Project of Nanyang Normal University (SYKF2018081, 2020STP006, 2020QN036 and 2020QN045).

Compliance with ethical standards

Conflict of interest The authors declare that they have no conflict of interest.

Publisher's note Springer Nature remains neutral with regard to jurisdictional claims in published maps and institutional affiliations.

References

1. Alzheimer's Disease International. World Alzheimer Report 2019: Attitudes to dementia. London: Alzheimer's Disease International; 2019. https://www.alz.co.uk/research/world-report-2019.
2. Citron M. Alzheimer's disease: strategies for disease modification. Nat Rev Drug Discov. 2010;9:387–98. https://doi.org/10.1038/nrd2896.
3. Fang J, Li Y, Liu R, Pang X, Li C, Yang R. et al. Discovery of multitarget-directed ligands against Alzheimer's disease through systematic prediction of chemical-protein interactions. J Chem Inf Model. 2015;55:149–64. https://doi.org/10.1021/ci500574n.
4. Zhang P, Xu S, Zhu Z, Xu J. Multi-target design strategies for the improved treatment of Alzheimer's disease. Eur J Med Chem. 2019;176:228–47. https://doi.org/10.1016/j.ejmech.2019.05.020.
5. de Freitas Silva M, Dias KST, Gontijo VS, Ortiz CJC, Viegas CJ. Multi-target directed drugs as a modern approach for drug design towards Alzheimer's disease: an update. Curr Med Chem. 2018;25:3491–525. https://doi.org/10.2174/0929867325666180111101843.
6. Cummings J, Lee G, Ritter A, Sabbagh M, Zhong K. Alzheimer's disease drug development pipeline: 2019. Alzheimers Dement (N. Y). 2019;5:272–93. https://doi.org/10.1016/j.trci.2019.05.008.
7. Sun BL, Li WW, Zhu C, Jin WS, Zeng F, Liu YH, et al. Clinical research on Alzheimer's disease: progress and perspectives. Neurosci Bull. 2018;34:1111–8. https://doi.org/10.1007/s12264-018-0249-z.
8. Hardy J, Selkoe DJ. The amyloid hypothesis of Alzheimer's disease: progress and problems on the road to therapeutics. Science 2002;297:353–6. https://doi.org/10.1126/science.1072994.
9. Nalivaeva NN, Turner AJ. Targeting amyloid clearance in Alzheimer's disease as a therapeutic strategy. Br J Pharm. 2019;176:3447–63. https://doi.org/10.1111/bph.14593.

10. Diomede L, Romeo M, Rognoni P, Beeg M, Foray C, Ghibaudi E, et al. Cardiac light chain amyloidosis: the role of metal ions in oxidative stress and mitochondrial damage. Antioxid Redox Signal. 2017;27:567–82. https://doi.org/10.1089/ars.2016.6848.
11. Cheignon C, Tomas M, Bonnefont-Rousselot D, Faller P, Hureau C, Collin F. Oxidative stress and the amyloid beta peptide in Alzheimer's disease. Redox Biol. 2018;14:450–64. https://doi.org/10.1016/j.redox.2017.10.014.
12. Schedin-Weiss S, Inoue M, Hromadkova L, Teranishi Y, Yamamoto NG, Wiehager B, et al. Monoamine oxidase B is elevated in Alzheimer disease neurons, is associated with γ-secretase and regulates neuronal amyloid β-peptide levels. Alzheimers Res Ther. 2017;9:57 https://doi.org/10.1186/s13195-017-0279-1.
13. Chang Y, Wang LB, Li D, Lei K, Liu SY. Efficacy of rasagiline for the treatment of Parkinson's disease: an updated meta-analysis. Ann Med. 2017;49:421–34. https://doi.org/10.1080/07853890.2017.1293285.
14. Özil M, Balaydın HT, Şentürk M. Synthesis of 5-methyl-2,4-dihydro-3H-1,2,4-triazole-3-one's aryl Schiff base derivatives and investigation of carbonic anhydrase and cholinesterase (AChE, BuChE) inhibitory properties. Bioorg Chem. 2019;86:705–13. https://doi.org/10.1016/j.bioorg.2019.02.045.
15. Riazimontazer E, Sadeghpour H, Nadri H, Sakhteman A, Tüylü Küçükkılınç T, Miri R, et al. Design, synthesis and biological activity of novel tacrine-isatin Schiff basehybrid derivatives. Bioorg Chem. 2019;89:103006 https://doi.org/10.1016/j.bioorg.2019.103006.
16. Jadhao M, Das C, Rawat A, Kumar H, Joshi R, Maiti S, et al. Development of multifunctional heterocyclic Schiff base as a potential metal chelator: a comprehensive spectroscopic approach towards drug discovery. J Biol Inorg Chem. 2017;22:47–59. https://doi.org/10.1007/s00775-016-1407-2.
17. Zanon VS, Lima JA, Cuya T, Lima FRS, da Fonseca ACC, Gomez JG, et al. In-vitro evaluation studies of 7-chloro-4-aminoquinoline Schiff bases and their copper complexes as cholinesterase inhibitors. J Inorg Biochem. 2019;191:183–93. https://doi.org/10.1016/j.jinorgbio.2018.11.019.
18. Tok F, Koçyiğit-Kaymakçıoğlu B, Sağlık BN, Levent S, Özkay Y, Kaplancıklı ZA. Synthesis and biological evaluation of new pyrazolone Schiff bases as monoamine oxidase and cholinesterase inhibitors. Bioorg Chem. 2019;84:41–50. https://doi.org/10.1016/j.bioorg.2018.11.016.
19. Sang Z, Wang K, Zhang P, Shi J, Liu W, Tan Z. Design, synthesis, in-silico and biological evaluation of novel chalcone derivatives as multi-function agents for the treatment of Alzheimer's disease. Eur J Med Chem. 2019;180:238–52. https://doi.org/10.1016/j.ejmech.2019.07.021.
20. Bai P, Wang K, Zhang P, Shi J, Cheng X, Zhang Q, et al. Development of chalcone-O-alkylamine derivatives as multifunctional agents against Alzheimer's disease. Eur J Med Chem. 2019;183:111737. https://doi.org/10.1016/j.ejmech.2019.111737.
21. Sang Z, Wang K, Shi J, Cheng X, Zhu G, Wei R, et al. Apigenin-rivastigmine hybrids as multi-target-directed liagnds for the treatment of Alzheimer's disease. Eur J Med Chem. 2020;187:111958 https://doi.org/10.1016/j.ejmech.2019.111958.
22. Sang Z, Wang K, Shi J, Liu W, Cheng X, Zhu G, et al. The development of advanced structural framework as multi-target-directed ligands for the treatment of Alzheimer's disease. Eur J Med Chem. 2020;192:112180. https://doi.org/10.1016/j.ejmech.2020.112180.
23. Di L, Kerns EH, Fan K, McConnell OJ, Carter GT. High throughput artificial membrane permeability assay for blood-brain barrier. Eur J Med Chem. 2003;38:223–32. https://doi.org/10.1016/s0223-5234(03)00012-6.
24. Sang Z, Wang K, Bai P, Wu A, Shi J, Liu W, et al. Design, synthesis and biological evaluation of novel *O*-carbamoyl ferulamide derivatives as multi-target-directed ligands for the treatment of Alzheimer's disease. Eur J Med Chem. 2020;194:112265. https://doi.org/10.1016/j.ejmech.2020.112265.
25. Pérez-Cruz F, Vazquez-Rodriguez S, Matos MJ, Herrera-Morales A, Villamena FA, Das A, et al. Synthesis and electrochemical and biological studies of novel coumarin-chalcone hybrid compounds. J Med Chem 2013;56:6136–45. https://doi.org/10.1021/jm400546y.